www.czasopisma.pan.pl PAN POLSKA AKADEMIA NAUK www.journals.pan.pl

Arch. Min. Sci. **69** (2024), 2, 159-174

Electronic version (in color) of this paper is available: http://mining.archives.pl

DOI: https://doi.org/10.24425/ams.2024.150339

ANDRZEJ PYTLIK[1*], WITOLD FRĄC[1]

INJECTION MICROPILE BAR FATIGUE RESISTANCE AT LOADS LOWER AND GREATER THAN THE YIELD STRENGTH OF STEEL

One of the techniques commonly applied today for deep foundation construction is based on self-drilling injection micropiles. Micropiles are structural elements intended primarily for reinforcing foundations and buildings, particularly under difficult terrain conditions. The goal of the tests presented herein is to inspect the fatigue resistance, strength and ductility of injection micropiles formed from 28Mn6 steel at loads significantly exceeding the values defined for the fatigue test in the requirements of the relevant European Assessment Document (EAD). The test results and the micropile bar strain model ε_M presented in this paper are primarily of interest to designers for the purposes of determining the fatigue resistance of steel micropiles, which find particular application in land degraded by mining activity that is characterised by frequent terrain vibration and mining-induced tremors.

None of the R25N injection micropile bars failed during the fatigue resistance testing at $2 \cdot 10^6$ cycles at a load $F_u = 0.7 \cdot F_{Re0.2}$ (under the yield strength of the 28Mn6 steel) as well as at $F_u = 1.0 \cdot F_{Re0.2}$ and $F_u = 1.2 \cdot F_{Re0.2}$, where the bars operated at the limit of and significantly above the load $F_{Re0.2}$ which results in stress at the yield point of the 28Mn6 steel. Furthermore, the bar tests conducted at static and cyclic loading demonstrated the high strength and good ductility of the 28Mn6 steel.

Keywords: self-drilling injection micropiles; bar fatigue resistance; strength and ductility of 28Mn6 steel; bar strain model

1. Introduction

The necessity to construct buildings and land transport infrastructure elements under difficult geological and engineering conditions, posed by factors such as weak soil with high deformability as well as concentrated vertical and horizontal loads imposed on the ground by various

[1] CENTRAL MINING INSTITUTE GIG, DEPARTMENT OF MECHANICAL DEVICES TESTING AND ROCKS, PLAC GWARKÓW 1, 40-166, KATOWICE, POLAND

* Corresponding author: ja.pytlik@gmail.co

structures, has resulted in the development of various techniques for deep foundation construction [1-3]. Setting structures and transportation networks on pile foundations is currently carried out by means of specialist foundation engineering techniques using piles produced from various materials, whose primary purpose is to transfer the static and dynamic loads to the deeper layers of the ground. One of the techniques commonly applied today for deep foundation construction is based on self-drilling injection micropiles. Micropiles (also known as small diameter piles) are structural elements intended primarily for reinforcing foundations and structures, particularly under difficult terrain conditions [1,4-6]. The basic requirements for micropiles are included in standards: PN-EN 1997-1:2008 [7] and PN-EN 14199:2015-07 [8] as well as European Assessment Documents EAD 200036-00-0103 [9] and ETAG 013 [10]. Standard PN-EN 1997-1:2008 [7] presents the general design principles in geotechnical work as per Eurocode 7 [5], whereas standard PN-EN 14199:2015-07 [8] defines the principles for micropile execution, which apply to drilled micropiles with a shaft diameter no greater than 300 mm or driven piles with a shaft diameter no greater than 150 mm. According to the above standard, injection micropiles can be formed from steel or other reinforcement materials as well as grout, mortar or concrete, or a combination of these materials. Detailed requirements for injection micropiles are provided in the European Assessment Documents EAD 200036-00-0103 [9] and ETAG 013 [10], which state that steel micropile elements, such as bars (hollow bars of seamless steel tubes) with nuts as well as ducts for coupling the bars, should be able to sustain $2 \cdot 10^6$ cycles of cyclic loading with a frequency of up to 10 Hz without failure. Guide values of strength of the hollow bar are: $R_{p0.2} \geq 450$ MPa (Characteristic yield strength), $R_m \geq 600$ MPa (Characteristic tensile strength), $A_{gt} \geq 5.0\%$ (Characteristic elongation at ultimate force) [9]. On the market, you can meet micropile bars made of such steel grades as: 28Mn6, S460 NH and S460 NLH.

In practice, micropiles transfer both static as well as dynamic loads, induced for example by: vibration generated by wind towers and their foundations [11], wind turbulence affecting bridges and their foundations [12] or car and rail transport affecting micropile-reinforced embankments [13]. Ground vibration is also present in mining areas where rock mass tremors result in great difficulties in maintaining structures and transportation networks [1,14]. Mining activity exerts a negative influence both on the surface, provoking the generation of continuous and discontinuous deformations, as well as on structures and transportation networks [15-21]. Discontinuous deformations generated on the surface of mining areas are one of the primary causes of damage to roads and highways, which also produce additional surface vibrations as a result of car traffic. Thus foundation system elements such as steel micropiles and soil nails are exposed to the influence of ground vibration-induced cyclic loads as well, therefore these elements should also be characterised by resistance to cyclic loading. This paper presents the laboratory test results of fatigue load resistance for injection micropiles formed from 28Mn6 steel. 28Mn6 steel is classified as a heat-treatable unalloyed steel [22-24], and it finds common application in the production of micropiles and soil nails by various manufacturers [25] as well as in the machine and automotive industries.

The goal of the tests presented herein is to inspect the strength and ductility of injection micropiles formed from 28Mn6 steel at loads significantly exceeding the values defined for the fatigue test in the requirements of the European Assessment Document EAD 200036-00-0103 [9]. Considering that micropiles can operate under variable static and cyclic loading as a result of mining damage-induced terrain surface degradation, the micropile fatigue strength testing was carried out for three load conditions relative to the yield strength of the steel: $0.7 \cdot F_{Re0.2}$ (per the requirements of EAD 200036-00-0103 [9], $1.0 \cdot F_{Re0.2}$ and $1.2 \cdot F_{Re0.2}$. Stress – strain relations

at static and cyclic loads were determined for comparative purposes. Stress – time relations for fatigue tests at fatigue loads $1.0 \cdot F_{Re0.2}$ and $1.2 \cdot F_{Re0.2}$ were determined as well, which served as the basis for defining the mathematical strain models ε_M of the 28Mn6 steel. Determining the fatigue strength of steel injection micropile bars is of key significance to the durability of structures and transportation networks.

2. Materials and methods

2.1. Materials

The tests encompassed the bars of SDA R25N injection micropiles formed from 28Mn6 steel (heat treatment: as-rolled condition (INSPECTION-CERTIFICATE 3.1 NO. 163019 [26], constituting the elements of a self-drilling nail and injection micropile system, whose technical parameters according to the manufacturer's data are presented in TABLE 1.

TABLE 1

Technical parameters of SDA R25N injection micropiles according to MINOVA ARNALL Sp. z o.o.

No.	Parameter	Unit	Type of micropile
			SDA R25N
1	Nominal diameter D_n	mm	25
2	Internal diameter D_i	mm	14
3	Nominal cross-sectional area S_0	mm^2	300
4	Nominal mass m	kg/m	2.35
5	Nominal yield load capacity $F_{p0.2}$	kN	150
6	Ultimate load capacity F_m	kN	200
7	Type of steel	—	28Mn6
8	Thread type (ISO 10208:1991)	—	R25LH
9	Yield strength $R_{p0.2}$	MPa	500
10	Tensile strength R_m	MPa	670
11	Resistance to fatigue	load cycles	$2 \cdot 10^6$
12	Stress range (fatigue test)	MPa	80
13	Upper load in the fatigue test $F_u = 0.7 \times F_{p0.2}$	kN	105

Apart from applications in micropile bars and soil nails, the 28Mn6 steel also finds use in the machine industry for producing elements such as: bolts, pins, axles, shafts and gears [27]. The 28Mn6 steel is also used for welded constructions [28], tubing [29] and in car suspension systems [30-34], where elements such as shock dampers, rods and arms are exposed to the influence of fatigue loads. The SDA R25N injection micropile bars were formed from steel tubes, whose technical parameters as well as the mechanical properties of the 28Mn6 steel were confirmed by a certificate (Inspection – Certificate 3.1 No. 163019, Voestalpine Tubulars GmbH & Co KG, Austria [26]):

- nominal pipe diameter and wall thickness: Ø24.7×5.5 mm,
- R25 left-hand rope thread (per ISO 10208:1991 [35]) over the entire bar length, with an outer diameter $d = 24.47^{0}_{-0.2}$ mm,

– yield strength $R_{p0.2}$ = 495±4 MPa,
– tensile strength R_m = 744±2 MPa,
– elongation A = 22±1%,
– the chemical composition of the 28Mn6 steel is presented in TABLE 2.

TABLE 2

The chemical composition of the 28Mn6 steel used to form the SDA R25N micropile tubes

C	Si	Mn	P	S	Cr	Ni	Cu
0.3054	0.1960	1.3557	0.0193	0.009	0.3433	0.1224	0.2110
Al	**Ti**	**Mo**	**V**	**Sn**	**B**	**N2**	**Nb**
0.0250	0.0114	0.0308	0.0050	0.0104	0.0004	0.0078	0.0022

2.2. Test methodology

The steel injection micropile bar test methodology encompassed three stages:

I. Micropile bar breaking strength tests at static loading (a total of four pieces of micropile bars with a total length of 1 m) per the load case in Fig. 1. During the tests, double nuts (hexagonal nut: thickness H = 35 mm, width across flats F = 41 mm, width across corners G = 47 mm) were applied to both ends of the bar to ensure a more uniform distribution of the load on the bar, to avoid local thread deformations and to minimise play typical of threaded couplings. In actual in situ micropile applications, one hex nut is usually used at the end of the micropile bar.

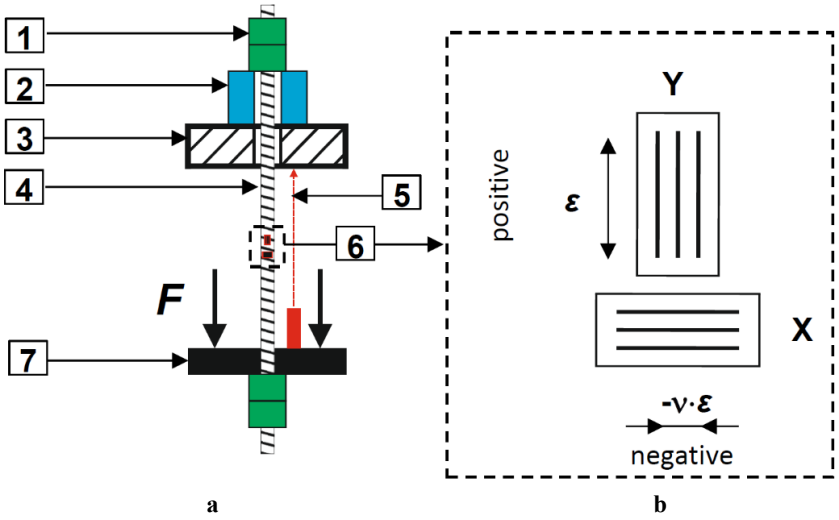

Fig. 1. Micropile bar load case (a) at static loading, and diagram of strain gauges (b) attached to the bar in an X-Y arrangement (strain gauge measuring circuits placed at an angle of 90º towards each other): 1 – two nuts on the bar, 2 – force sensor, 3 – fixed testing machine crosshead, 4 – micropile bar, 5 – laser displacement sensor, 6 – strain gauges for measuring the bar strain e, 7 – moving testing machine crosshead applying a load on the bar

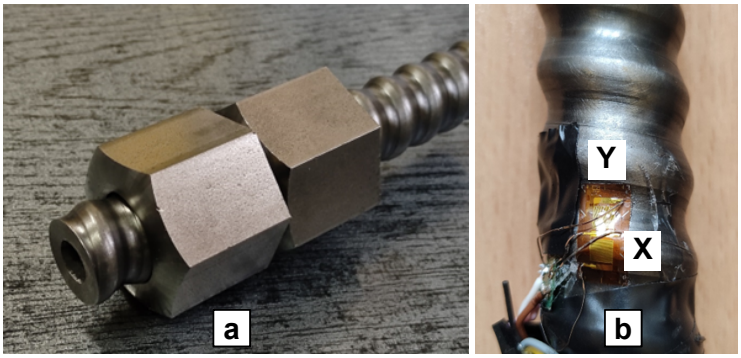

Fig. 2. View of the SDA R25N micropile bar with double nuts at the end (a) and view of the bar with an attached rosette of two strain gauges placed at an angle of 0° (Y) and 90° (X) relative to the bar axis

The tests were conducted to inspect the mechanical properties of the steel and the bar load capacity at static tensile loading until failure.

II. Strength tests at cyclic tensile fatigue loading per the load case in Fig. 3.

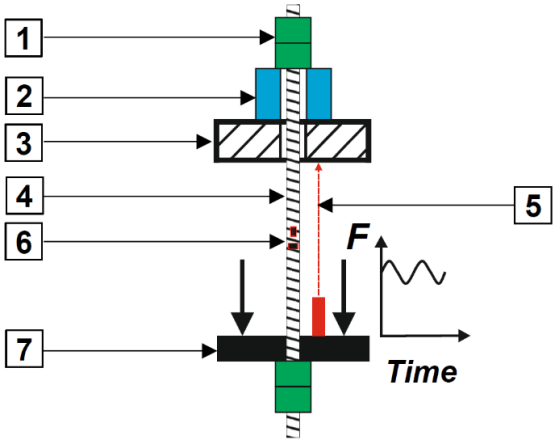

Fig. 3. Micropile bar load case at cyclic loading, with strain gauges attached to the bar in an X-Y arrangement (strain gauge measuring circuits placed at an angle of 90° towards each other): 1 – two nuts on the bar, 2 – force sensor, 3 – fixed testing machine crosshead, 4 – micropile bar, 5 – laser displacement sensor, 6 – strain gauges for measuring the bar strain ε, 7 – moving testing machine crosshead applying a load on the bar

The micropile bar fatigue strength (a total of six pieces of micropile bars with a total length of 1.4 m – two pieces for each load condition) was investigated for three load conditions F_u (upper load in the fatigue test) relative to the yield strength of the steel:

1) $0.7 \cdot R_{p0.2} = 105$ kN ($R_{p0.2} = 150$ kN – nominal yield load capacity per the manufacturer's catalogue data (TABLE 1) – according to the requirements of EAD 200036-00-0103 [9]),

2) $1.0 \cdot R_{p0.2} = 190$ kN – $R_{p0.2}$ is the value of the force generating stress at the yield point of the steel used to form the R25N micropile bars, determined during bar breaking laboratory tests at static loading,
3) $1.2 \cdot R_{p0.2} = 228$ kN.

III. Micropile bar breaking strength tests at static loading per the load case in Fig. 1 after carrying out fatigue strength testing per the load case in Fig. 3. The purpose of these tests was to inspect the variations in the strength characteristics of the steel that had occurred as a result of the cyclic load applied to the bars and to compare them with the characteristics of the steel determined during bar breaking at static loading.

Stress – strain relations at static and cyclic loads were determined during the tests for comparative purposes. Stress – time relations for fatigue tests at fatigue loads $1.0 \cdot R_{p0.2}$ and $1.2 \cdot R_{p0.2}$ were determined as well, which served as the basis for defining the mathematical strain models of the 28Mn6 steel. The micropile bar tests were carried out by means of a ZD-100 Pu testing machine with a nominal static loading range of up to 1000 kN and a fatigue loading range of up to 550 kN. The testing machine was equipped with an HBK QuantumX MX840B measurement amplifier connected to force and displacement transducers as well as strain rosettes for measuring the bar strain. The force F loading the micropile bar was measured using an HBK C6A strain gauge sensor with a measuring range of 2 MN (class 0.5), while the bar elongation L was measured through a SENSOPART FT 80 RLA-500 laser sensor with a measuring range of up to 500 mm, a resolution of 0.5 mm and a response time of 0.4 ms. The bar strain ε was measured by means of strain gauges (SG in short) operating as a Wheatstone half bridge circuit, which enabled the compensation of temperature during extended fatigue tests. The $1.0 \cdot R_{p0.2}$ fatigue tests involved 1-XY11-3/350 strain rosettes (Y series with two measuring grids, 0°/90° T rosette / double SG), while the $1.2 \cdot R_{p0.2}$ fatigue tests employed 1-CXY31-3/350ZE rosettes (0°/90° T rosette / double SG). The static measurements were carried out with a sampling frequency $f_s = 50$ Hz, and the dynamic measurements with a sampling frequency $f_s = 300$ Hz. All the measurements were registered on a computer with the HBK CatmanAP software for purposes of control and interaction with the QuantumX MX840B amplifier as well as for data visualisation. The measurement data serve as the basis for determining the courses of force $F = f(t)$ and elongation $L = f(t)$ as functions of time, force as a function of elongation $F = f(L)$, stress as a function of strain $\sigma = f(\varepsilon)$ and strain as a function of time $\varepsilon = f(t)$, which are then used for further analysis and to determine the work applied to the deformed micropile bar. The total energy W consumed for the bar elongation is calculated by integrating the $F = f(L)$ relation:

$$W = \int_0^{L_t} F(L)\,dL, \ \text{J} \tag{2.1}$$

where: L_t – bar elongation at rupture, mm.

The calculated energy W does not constitute a material parameter, as it depends primarily on the cross-sectional area and length of the micropile bar. Specific energy W_v, which is the energy accumulated in a unit of volume of the bar as a result of its elasto-plastic deformations, can be used to compare the test results of bars formed from 28Mn6 steel with other grades of steel. The total specific energy W_v can be calculated using the following formula [36,37]:

$$W_v = \frac{W}{S_0 \cdot L_0}, \text{ kJ/dm}^3 \tag{2.2}$$

where:

S_0 – initial effective cross-sectional area of the micropile bar, mm^2,
L_0 – initial measuring length of the micropile bar, mm.

The initial effective cross-sectional area S_0 of the micropile bar is calculated using the following formula (PN-H-93215:1982 [38]):

$$S_0 = \frac{m_r}{\rho \cdot l_r} 10^6 = 127.4 \frac{m_r}{l_r}, \text{ mm}^2 \tag{2.3}$$

where:

l_r – length of the micropile bar sample, m,
m_r – mass of the micropile bar sample, kg,
r – density of steel (r = 7850 kg/m^3).

The average force F_a of the resistance posed by the micropile bar during its elongation over a section L_t can be used for comparative purposes, calculated using the following formula:

$$F_a = \frac{W}{L_t} \tag{2.4}$$

After rupture of the micropile sample, the value of relative constriction Z is also calculated, which determines the reduction in the cross-sectional area of the sample S_u at the point of sample rupture, with respect to the area of the original cross-section area S_0:

$$Z = \frac{S_0 - S_u}{S_0} \cdot 100\% \tag{2.5}$$

2.3. Mathematical model of steel micropile bar strain during fatigue testing

The courses of strain as a function of time $\varepsilon = f(t)$ determined based on the fatigue tests can be fitted to a mathematical model describing the course of the micropile bar test in the test setup at cyclic loading. Using the computer software OriginPro 6.1 by Microcal Software, Inc. [39], which includes a module for nonlinear function estimation, made it possible to fit the courses of the $\varepsilon = f(t)$ function to the mathematical model expressed with the following relationship:

$$\varepsilon_M = a\left(1 - e^{(-bt)}\right)^c \tag{2.6}$$

where:

ε_M – mathematical model of the micropile bar strain at cyclic loading during fatigue testing at 2×10^6 cycles, %,
a, b, c – parameters of the $\varepsilon_M = f(t)$ function.

The nonlinear estimation module in the ORIGIN software determines the general fitting procedure for estimating any type of relationship between a dependent variable and independent variables. The ORIGIN software utilises the Levenberg-Marquardt algorithm to calculate the function parameters using the method of least squares. The function defined by the equation per formula 2.6 corresponds to the Chapman-Richards function and constitutes a model of a predefined function (as a Chapman model) in the software's calculation module.

3. Results

Per the steel R25N micropile bar test methodology, stage I involved the static breaking tests of bars with an effective cross-sectional area S_0 = 305.7 mm^2 and an initial micropile bar measuring length L_0 = 500 mm. The results of these tests are presented in TABLE 3.

TABLE 3

Results of R25N micropile bar breaking tests at static loading

$F_{Re0.2}$, kN	F_{max}, kN	L_t, mm	F_t, kN	A_t, %	W, kJ	W_v, kJ/dm^3	F_a, kN	$R_{e0.2}$, MPa	R_m, MPa
191.5 ±4.6	232.3 ±1.0	44.8 ±5.0	208.7 ±1.3	9.0 ±1.0	9.205 ±1.137	60.223 ±7.440	205.3 ±3.4	626.5 ±15.0	760.0 ±3.3

Typical charts of force − elongation and stress – strain relations during the static R25N micropile bar breaking tests are presented in Fig. 4.

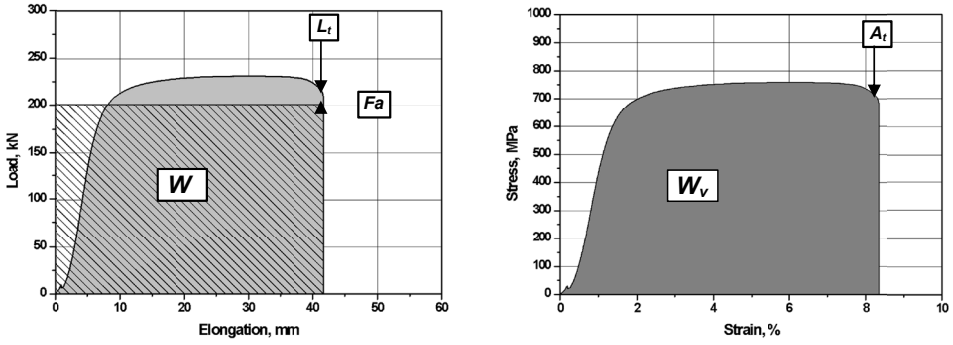

W – total energy consumed for the bar elongation; W_v – total specific energy; L_t – bar elongation at rupture; F_a – average force; A_t – bar strain at rupture

Fig. 4. Typical charts of force – elongation and stress – strain relations during static R25N micropile bar breaking tests

The results obtained for the steel R25N micropile bars during static breaking tests demonstrate that the technical parameters of the bars are higher than those declared by the Manufacturer in the catalogue data (TABLE 1). This is beneficial from the perspective of foundation construction safety, as the actual safety factor is greater than the designer's estimations. The value of the

force generating stress at the yield point of the steel bar is $F_{Re0.2}$ = 191.5±4.6 kN, whereas the effective cross-sectional area of the bar is S_0 = 305.7 mm^2, which exceeds the declared minimum catalogue data. The values $F_{Re0.2}$ = 190 kN and S_0 = 305.7 mm^2 were adopted for further fatigue test parameter determination.

The fatigue strength testing (stage II) of the steel bars at an upper load $F_u = 0.7 \cdot F_{p0.2}$ = 105 kN confirmed their fatigue resistance to $2 \cdot 10^6$ load cycles with a frequency of 10 Hz. None of the bars suffered failure during the fatigue tests. Fig. 5 presents typical charts of force – elongation and stress – strain relations determined during the static bar breaking tests (initial micropile bar measuring length was L_0 = 500 mm) after carrying out $2 \cdot 10^6$ load cycles with a frequency of 10 Hz, while the results of these tests are presented in TABLE 4.

TABLE 4

$F_{Re0.2}$, kN	F_{max}, kN	L_t, mm	F_t, kN	A_t, %	W, kJ	W_v, kJ/dm^3	F_a, kN	$R_{e0.2}$, MPa	R_m, MPa
186.20	236.0	41.9	214.5	8.4	8.774	57.400	209.1	609.1	772.1

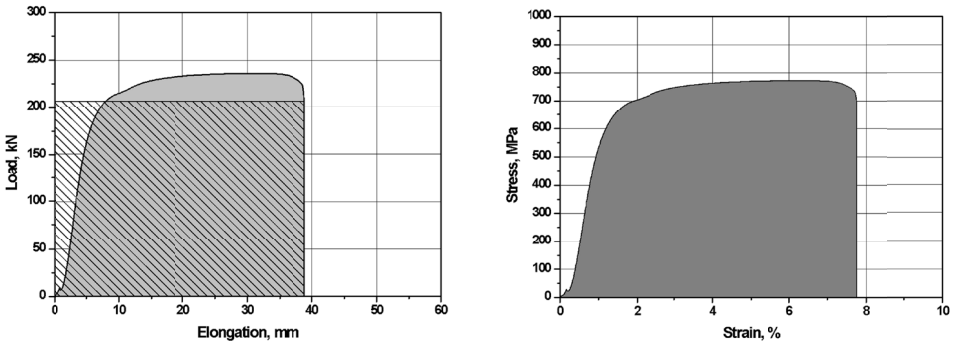

Fig. 5. Typical charts of force – elongation and stress – strain relations during static R25N micropile bar breaking tests after carrying out $2 \cdot 10^6$ load cycles at an upper force F_u = 105 kN (upper load in the fatigue test $F_u = 0.7 \cdot F_{p0.2}$)

The steel bar fatigue strength tests (initial micropile bar measuring length was L_0 = 1260 mm) at an upper load $F_u = 1.0 \cdot F_{Re0.2}$ = 190 kN and $F_u = 1.2 \cdot F_{Re0.2}$ = 228 kN also demonstrated the bars' resistance to $2 \cdot 10^6$ load cycles with a frequency of 10 Hz. The initial measuring length L_0 was extended to 1260 mm (relative to the previously presented test results) due to the application of an additional force transducer in the system (for additional control of the force value) as well as a laser displacement sensor (working range of 250-750 mm). None of the bars suffered failure during the fatigue tests. Fig. 6 presents a typical strain – time curve obtained from tests at $F_u = 1.0 \cdot F_{Re0.2}$ = 190 kN, while Fig. 7 presents charts of force – elongation and stress – strain relations determined during static bar breaking tests after carrying out $2 \cdot 10^6$ load cycles with a frequency of 10 Hz.

The results of R25N micropile bar breaking tests at static loading after carrying out $2 \cdot 10^6$ load cycles at F_u = 190 kN with a frequency of 10 Hz are presented in TABLE 5, while a typical post-test view of a ruptured bar is displayed in Fig. 8.

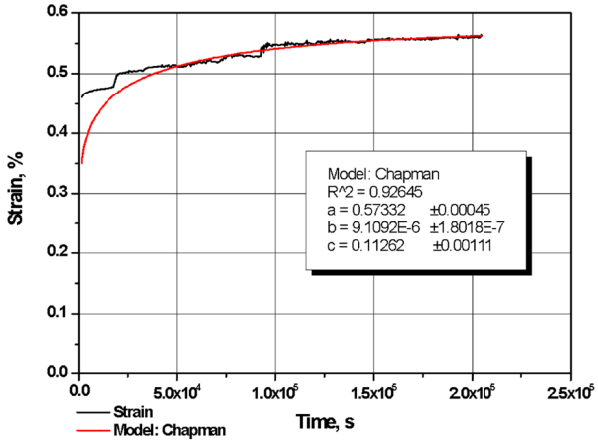

Fig. 6. $\varepsilon = f(t)$ relation chart and mathematical model in the form of a Chapman – Richards function during R25N micropile bar fatigue strength testing at an upper force $F_u = 1.0 \cdot F_{Re0.2} = 190$ kN (cyclic loading range: 166-190 kN corresponding to the stress range of 80 MPa defined in EAD [9])

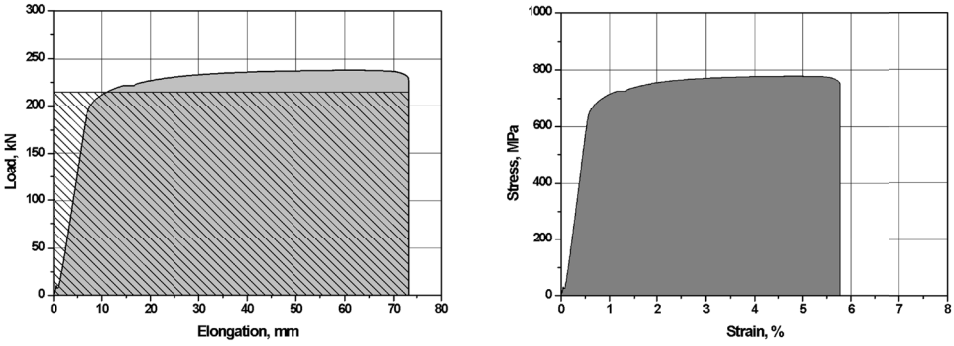

Fig. 7. Typical charts of force – elongation and stress – strain relations during static R25N micropile bar breaking tests after carrying out $2 \cdot 10^6$ load cycles at $F_u = 1.0 \cdot F_{Re0.2} = 190$ kN (upper load in the fatigue test $F_u = 1.0 \cdot F_{Re0.2}$)

TABLE 5

Results of R25N micropile bar breaking tests at static loading after carrying out $2 \cdot 10^6$ load cycles at $F_u = 190$ kN with a frequency of 10 Hz

$F_{Re0.2}$, kN	F_{max}, kN	L_t, mm	F_t, kN	A_t, %	W, kJ	W_v, kJ/dm^3	F_a, kN	$R_{e0.2}$, MPa	R_m, MPa
212.1	237.8	73.0	227.5	5.8	15.676	40.605	214.7	693.9	778.0

The results of R25N micropile bar breaking tests at static loading after carrying out $2 \cdot 10^6$ load cycles at $F_u = 1.2 \cdot F_{Re0.2} = 228$ kN with a frequency of 10 Hz are presented in TABLE 6, while Fig. 9 displays a typical strain – time curve, and Fig. 10 demonstrates charts of force – elongation and stress – strain relations. A typical post-test view of a ruptured bar is presented in Fig. 11.

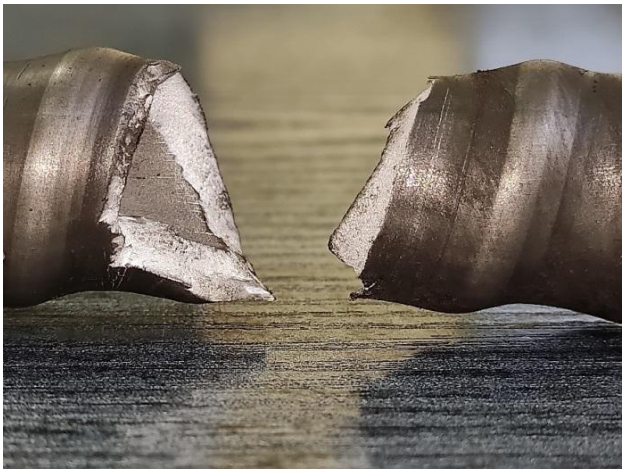

Fig. 8. Typical view of a ruptured R25N micropile bar at static loading after carrying out $2 \cdot 10^6$ load cycles at an upper force $F_u = 190$ kN (upper load in the fatigue test $F_u = 1.0 \cdot F_{Re0.2}$). The relative constriction of the cross-section of the micropile bar at the point of rupture is approximately $Z \approx 31.3\%$

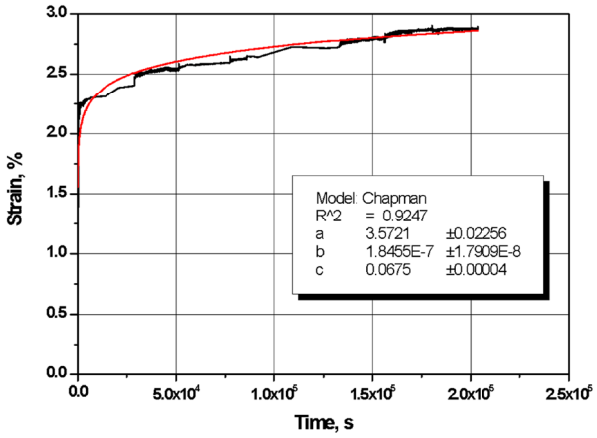

Fig. 9. $\varepsilon = f(t)$ relation chart and mathematical model in the form of a Chapman – Richards function during R25N micropile bar fatigue strength testing at an upper force $F_u = 1.2 \cdot F_{Re0.2} = 228$ kN (cyclic loading range: 204-228 kN corresponding to the stress range of 80 MPa defined in EAD [9])

TABLE 6

Results of R25N micropile bar breaking tests at static loading after carrying out $2 \cdot 10^6$ load cycles at $F_u = 228$ kN with a frequency of 10 Hz

$F_{Re0.2}$, kN	F_{max}, kN	L_t, mm	F_t, kN	A_t, %	W, k J	W_v, kJ/dm^3	F_a, kN	$R_{e\,0.2}$, MPa	R_m, MPa
236.9	241.5	55.9	222.0	4.38	12.400	31.774	221.8	775.0	789.9

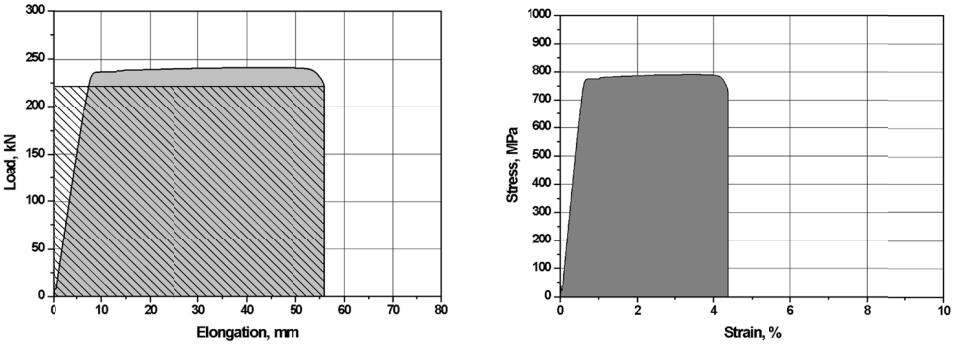

Fig. 10. Typical charts of force-elongation and stress-strain relations during static R25N micropile bar breaking tests after carrying out $2 \cdot 10^6$ load cycles at $F_u = 1.2 \cdot F_{Re0.2} = 228$ kN (upper load in the fatigue test $F_u = 1.2 \cdot F_{Re0.2}$)

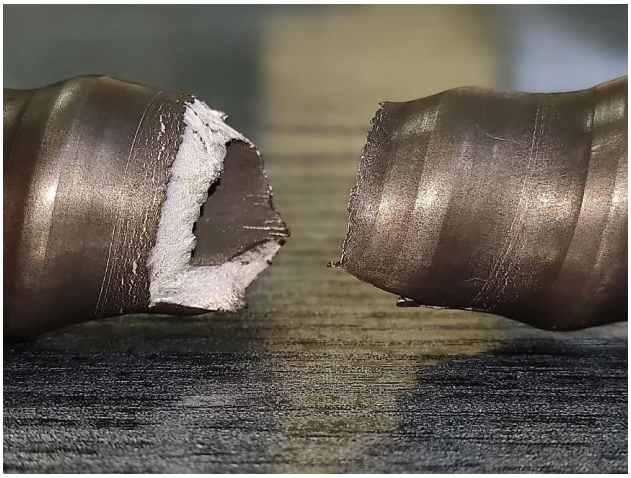

Fig. 11. Typical view of a ruptured R25N micropile bar at static loading after carrying out $2 \cdot 10^6$ load cycles at an upper force $F_u = 228$ kN (upper load in the fatigue test $F_u = 1.2 \cdot F_{Re0.2}$). The relative constriction of the cross section of the micropile bar at the point of rupture is approximately $Z \approx 34.9\%$

4. Discussion

The chart of the $\varepsilon = f(t)$ relation and its mathematical model in the form of a Chapman-Richards function determined during the fatigue testing of R25N micropile bars at an upper force $F_u = 1.0 \cdot F_{Re0.2} = 190$ kN demonstrate that after carrying out $2 \cdot 10^6$ load cycles at $F_u = 1.2 \cdot F_{Re0.2} = 190$ kN with a frequency of 10 Hz, the strain ε reached a value of about 0.563%. Analysing the mathematical model of the Chapman-Richards $\varepsilon_M = f(t)$ function (per formula 2.6) demonstrates that the continued course of the function (above $2 \cdot 10^6$ load cycles) becomes asymptotically close to the value of strain corresponding closely to the parameter $a = 0.573$, which shows that the continued strengthening of the 28Mn6 steel will undergo a slight build-up.

The $\varepsilon = f(t)$ relation chart and its mathematical model in the form of a Chapman-Richards function determined during the R25N micropile bar fatigue strength testing at an upper force $F_u = 1.2 \cdot F_{Re0.2} = 228$ kN exhibits a different character. After carrying out $2 \cdot 10^6$ load cycles at $F_u = 1.2 \cdot F_{Re0.2} = 228$ kN with a frequency of 10 Hz, the strain ε reached a value of about 2.878%. Analysing the mathematical model of the Chapman-Richards $\varepsilon_M = f(t)$ function (per formula 2.6) demonstrates that the continued course of the function after a time of $2 \cdot 10^5$ s (which corresponds to $2 \cdot 10^6$ load cycles with a frequency of 10 Hz) becomes asymptotically close to the value of strain corresponding closely to the parameter $a = 3.572$, which shows that the strain of the 28Mn6 steel will continue to grow, and its estimated value of about $\varepsilon = 3.57\%$ will be reached only after a time of about $2 \cdot 10^7$ s.

The typical charts of force – elongation and stress – strain relations presented in Fig. 5, determined during static R25N micropile bar breaking tests (after carrying out $2 \cdot 10^6$ load cycles with a frequency of 10 Hz), exhibit no significant differences from the relation charts determined for the bars not subjected to the fatigue tests (Fig. 4). On the other hand, the charts of force – elongation and stress – strain relations presented in Fig. 7 and 10, determined during static R25N micropile bar breaking tests after carrying out $2 \cdot 10^6$ load cycles with a frequency of 10 Hz, exhibit significant differences from the relation charts determined for the bars not subjected to the fatigue tests. The force-generating stress at the yield point $F_{Re0.2} = 191.5 \pm 4.6$ kN and the elongation at rupture $A_t = 9.0 \pm 1.0\%$ determined during bar tests at static loading (bar samples not subjected to prior fatigue testing) after fatigue tests at $F_u = 1.0 \cdot F_{Re0.2} = 190$ kN underwent changes: $F_{Re0.2}$ increased by about 11% while the elongation A_t decreased by about 36%. In the case of fatigue tests at $F_u = 1.2 \cdot F_{Re0.2} = 228$ kN, the force-generating stress at the yield point increased by about 24% while the elongation at rupture decreased by about 51% relative to the bars tested during static trials, which were not subjected to prior fatigue testing. These variations also exhibit an influence on the values of work W and W_v. This is particularly visible when analysing the specific work W_v (TABLES 3-6), which underwent a systematic decrease during consecutive tests. At the same time, as a result of the strengthening of steel during fatigue testing, the values of maximum $F_{\max}$ and average F_a force increased as follows: $F_{\max}$ by about 2% (at $F_u = 1.0 \cdot F_{Re0.2}$) and 4% (at $F_u = 1.2 \cdot F_{Re0.2}$), and F_a by about 5% (at $F_u = 1.0 \cdot F_{Re0.2}$) and 8% (at $F_u = 1.2 \cdot F_{Re0.2}$).

What is characteristic is that the charts of force – elongation and stress – strain relations exhibit steep build-ups of the force $F_{Re0.2}$ and stress $R_{e0.2}$ to values close to the maximum force and stress, giving the charts a shape similar to that of a trapezoid.

The performed tests proved the high fatigue strength of the 28Mn6 steel at loads below, equal to and 20% greater than its yield strength. The testing also demonstrated the good ductility of the steel, as exhibited by the values of the bar strain after tests performed at static and cyclic loading. The concerns voiced in literature [40,41] regarding the use of the heat treated 28Mn6 steel for producing soil nails and micropile bars in the context of its inadequate ductility, found no confirmation during the tests.

The developed mathematical strain models ε_M determined for $F_u = 1.0 \cdot F_{Re0.2}$ and $F_u = 1.2 \cdot F_{Re0.2}$ demonstrates good conformity with the actual values obtained during the experiments. However, it is difficult to make a reference to any results provided in literature, as the authors of this paper found no similar tests that would determine strain – time relations during fatigue testing performed for upper cyclic load values F_u equal to or significantly exceeding the values of forces generating stresses at the yield point of the 28Mn6 steel or its counterparts.

The research results presented in the article only partially fill a research gap. Currently, it is too early, for example, to make comparisons as to the differences between micropile bar deformation induced by static loading and cyclic loading.

5. Conclusions

During the fatigue tests of R25N injection micropile bars, both at an upper cyclic load $F_u = 0.7 \cdot F_{Re0.2}$, where the bars operated within the limits of the yield strength of the 28Mn6 steel, as well as at $F_u = 1.0 \cdot F_{Re0.2}$ and $F_u = 1.2 \cdot F_{Re0.2}$, where the bars operated at and above the yield strength of the 28Mn6 steel, none of the bars suffered failure. The bar tests conducted at static and cyclic loads demonstrated the high strength and good ductility of the 28Mn6 steel. It can therefore be concluded that the steel bars of the R25N self-drilling injection micropiles can be useful for reinforcing foundations and structures under difficult terrain conditions, where the micropiles may be exposed to loads significantly exceeding those defined for fatigue testing in the requirements of the European Assessment Document EAD 200036-00-0103 [9]. The developed bar strain model ε_M can be of use to designers for the purposes of determining the resistance of steel micropiles applied particularly in land degraded by mining activity that is characterised by frequent terrain vibration and mining-induced tremors. In areas degraded by mining activities, there are plans to perform in situ monitoring of steel micropile bars to determine actual values of stresses and deformations of the rock and soil subsoil.

Acknowledgements

The tests were performed in the framework of the research work in the Central Mining Institute [No. 11384011-180] and was financially supported by the Polish Ministry of Education and Science.

References

[1] E. Stilger-Szydło, Posadowienia budowli infrastruktury transportu lądowego: teoria, projektowanie, realizacja, Dolnośląskie Wydawnictwo Edukacyjne (2005).

[2] K. Gwizdała, Fundamenty palowe. Tom 1. Technologie i obliczenia, Wydawnictwo Naukowe PWN, Warszawa (2013).

[3] K. Gwizdała, Fundamenty palowe. Tom 2. Badania i zastosowania, Wydawnictwo Naukowe PWN, Warszawa (2014).

[4] B. Kłosiński, Mikropale – stan techniki i perspektywy. Nowoczesne Budownictwo Inżynieryjne **3**, 72-76 (2011).

[5] B. Kłosiński, Zasady i problemy projektowania mikropali według Eurokodu 7. Geoinżynieria: drogi, mosty tunele **3**, 26-32 (2014).

[6] J. Bzówka, A. Juzwa, K. Knapik, K. Stelmach, Geotechnika komunikacyjna, Wydawnictwo Politechniki Śląskiej, Gliwice (2012).

[7] PN-EN 1997-1:2008. Eurocode 7: Geotechnical design – Part 1: General rules. Polski Komitet Normalizacyjny, (2008).

[8] PN-EN 14199:2015-07 – Execution of special geotechnical work – Micropiles. Polski Komitet Normalizacyjny, (2015).

[9] European Assessment Document EAD 200036-00-0103: Kit for micropiles – kit with hollow bars for self-drilling micropiles – hollow bars of seamples steel tubes, August (2016).

[10] European Organization for Technical Approvals, ETAG 013: Guideline for European Technical Approval of Post-Tensioning Kits for Prestressing of Structures, European Organization for Technical Approvals, Brussels, Belgium, (2002).

[11] R.P. Matos, P.L. Pinto, C.S. Rebelo, H.S. Gervásio, M. Veljkovic, Improved design of tubular wind tower foundations using steel micropiles. Structure and Infrastructure Engineering **12** (9), 1038-1050 (2016). DOI: https://doi.org/10.1080/15732479.2015.1076853

[12] J. Berthellemy, G. Seidl, W. Lorenc, Recent Structures and Bridges built with the CL Steel-concrete Connection. Tomorrow's Megastructures. 40th IABSE Symposium, 19-21 September 2018, Nantes, France 2-51 (2018). DOI: https://doi.org/10.2749/nantes.2018

[13] N. Maca, Nowoczesne rozwiązania geotechniczne w odpowiedzi na wyzwania budownictwa kolejowego. Zeszyty Naukowo-Techniczne Stowarzyszenia Inżynierów i Techników Komunikacji w Krakowie. Seria: Materiały Konferencyjne **2** (123), 397-409 (2021). https://yadda.icm.edu.pl/baztech/element/bwmeta1.element.baztech-232b026e-7b32-4483-b6fe-17cdf01bb0a3, accessed: 20.05.2022

[14] J. Dubiński, G. Mutke, J. Chodacki, Distribution of peak ground vibration caused by mining induced seismic events in the Upper Silesian Coal Basin in Poland. Arch. Min. Sci. **65**, 3, 419-432 (2020). DOI: https://doi.org/10.24425/ams.2020.133200

[15] A. Kowalski, Deformacje powierzchni na terenach górniczych kopalń węgla kamiennego, Główny Instytut Górnictwa, Katowice (2020).

[16] A. Kotyrba, A. Kowalski, Linear discontinuous deformation of A4 highway within mining area 'Halemba'. Gospodarka Surowcami Mineralnymi **25** (3), 303-317 (2009).

[17] M. Grygierek, P. Kalisz, Influence of mining operations on road pavement and sewer system–selected case studies. Journal of Sustainable Mining **17** (2), 56-67 (2018). DOI: https://doi.org/10.46873/2300-3960.1122

[18] P. Kalisz, M. Zięba, M. Grygierek, Wpływ eksploatacji górniczej na uszkodzenia nawierzchni drogowych i rurociągów – wybrane przykłady. Przegląd Górniczy **76** (2), 29-35 (2020).

[19] M. Zięba, P. Kalisz, M. Grygierek, The impact of mining deformations on road pavements reinforced with geosynthetics. Archives of Mining Sciences **65** (4), 751-767 (2020). DOI: https://doi.org/10.24425/ams.2020.134145

[20] M. Grygierek, K.J. Sternik, Identification of Pavement Model Parameters in the Area of Discontinuous Surface Deformation Based on FWD Tests. International Journal of Civil Engineering **19** (3), 265-282 (2021). DOI: https://doi.org/10.1007/s40999-020-00563-y

[21] M. Wróblewska, M Grygierek, Assessment of Visual Representation Methods of Linear Discontinuous Deformation Zones in the Right-of-Way. Appl. Sci. **12** (5), 2538 (2022). DOI: https://doi.org/10.3390/app12052538

[22] L.A. Dobrzański, Podstawy nauki o materiałach i metaloznawstwo: materiały inżynierskie z podstawami projektowania materiałowego, Wydawnictwa Naukowo-Techniczne (2002).

[23] EN 10083-2:2006(E) – Steels for quenching and tempering – Part 2: Technical delivery conditions for non alloy steels.

[24] EN ISO 683-1:2016(E) – Heat-treatable steels, alloy steels and free-cutting steels – Part 1: Non-alloy steels for quenching and tempering.

[25] M. Topolnicki, R. Buca, D. Dymek, Bezpieczeństwo dużych i głębokich wykopów budowlanych. Nowoczesne Budownictwo Inżynieryjne **5**, 42-47 (2015). https://yadda.icm.edu.pl/baztech/element/bwmeta1.element.baztech-e7a5fdc2-5806-4ee3-9b9e-61fc9dddf194, accessed: 20.05.2022

[26] Inspection-Certificate 3.1 No. 163019 (2021). Pipe for Anchor R25N. Heat treatment: as-rolled condition. Manufacturer: Voestalpine Tubulars GmbH & Co KG, Austria.

[27] U. Fischer, R. Gomeringer, M. Heinzler, R. Kilgus, F. Näher, S. Oesterle, H. Paetzold, A. Stephan, Mechanical and Metal Trades Handbook. Polish edition by: dr hab. inż. Joachim Potrykus, prof. nadzw. Wydawnictwo REA s.j. (2008).

[28] T. Kovács, P. Pinke, BWRA and Séférian Model for Preheating Temperature Calculation in Case of Low Alloyed and Unalloyed Steel. Materials Science Forum, Trans. Tech. Publications Ltd. **885**, 239-244 (2017). DOI: https://doi.org/10.4028/www.scientific.net/msf.885.239

[29] K.E. Hensger, Processing of advanced structural steels on CSP plants. Metalurgija **41** (3), 183-190 (2002). https://hrcak.srce.hr/clanak/189888, accessed: 20.05.2022

[30] M. Melaika, S. Nagurnas, R. Pečeliūnas, N. Višniakov, G. Garbinčius, Investigation on distribution of stresses in steel and aluminium alloy arms of a car suspension system. Mechanika **19** (6), 632-640 (2013). DOI: https://doi.org/10.5755/j01.mech.19.6.5987

[31] M. Jimenez-Martinez, Manufacturing effects on fatigue strength. Engineering Failure Analysis **108**, 104339 (2020). DOI: https://doi.org/10.1016/j.engfailanal.2019.104339

[32] J.D. Almer, J.B. Cohen, B. Moran, The effects of residual macrostresses and microstresses on fatigue crack initiation. Materials Science and Engineering: A **284** (1-2), 268-279 (2000). DOI: https://doi.org/10.1016/S0921-5093(99)00779-0

[33] W.J. Kang, A.K. Kim, G.H. Kim, Fatigue failure prediction of press fitted parts subjected to a cyclic loading condition by finite element methods. Fatigue & Fracture of Engineering Materials & Structures **30** (12), 1194-1202 (2007). DOI: https://doi.org/10.1111/j.1460-2695.2007.01188.x

[34] E.S. Palma, E.D. Santos, Fatigue damage analysis in an automobile stabilizer bar. Proceedings of the Institution of Mechanical Engineers, Part D. Journal of Automobile Engineering **216** (11), 865-871 (2002). DOI: https://doi.org/10.1243/095440702321031414

[35] ISO 10208:1991 – Rock drilling equipment. Left-hand rope threads.

[36] N.M. Bielajew, Wytrzymałość materiałów, Wydawnictwo Ministerstwa Obrony Narodowej, Warszawa (1954).

[37] W. Domke, Vademecum materiałoznawstwa: stal, metale nieżelazne, tworzywa sztuczne, badania metali, Wydawnictwa Naukowo-Techniczne, Warszawa (1977).

[38] PN-H-93215:1982 – Walcówka i pręty stalowe do zbrojenia betonu. Polski Komitet Normalizacyjny, Warszawa (1982).

[39] Origin User's Manual. Version 6. Data Analysis and Technical Graphics Software. Microcal Software, Inc., Northampton, MA 01060, USA (1999).

[40] N. Maca, J. Sierant, Stal do zbrojenia mikropali i gwoździ gruntowych wykonywanych w technologii samowiercącej. Nowoczesne Budownictwo Inżynieryjne **4**, 60-64 (2016). https://yadda.icm.edu.pl/baztech/element/bwmeta1.element.baztech-e447421e-ab93-4475-b5e5-ccf9d01a4c80, accessed: 20.05.2022

[41] N. Maca, J. Sierant, Samowiercące systemy iniekcyjnych mikropali i gwoździ gruntowych. Wymagania techniczne i normowe dla zbrojenia do zastosowań trwałych. Zeszyty Naukowo-Techniczne Stowarzyszenia Inżynierów i Techników Komunikacji w Krakowie. Seria: Materiały Konferencyjne **2** (123), 411-427 (2021). https://yadda.icm.edu.pl/baztech/element/bwmeta1.element.baztech-bfa05634-f690-401f-ba0d-b6b03aa0cf06 (accessed: 20.05.2022)